01 Jan 2010

Effect Of Radar-rainfall Uncertainties On The Spatial Characterization Of Rainfall Events

Pradeep V. Mandapaka

Gabriele Villarini

Bong Chul Seo
Missouri University of Science and Technology, bongchul.seo@mst.edu

Witold F. Krajewski

Recommended Citation

P. V. Mandapaka et al., "Effect Of Radar-rainfall Uncertainties On The Spatial Characterization Of Rainfall Events," *Journal of Geophysical Research Atmospheres*, vol. 115, no. 17, article no. D17110, Wiley; American Geophysical Union, Jan 2010.
The definitive version is available at https://doi.org/10.1029/2009JD013366

Effect of radar-rainfall uncertainties on the spatial characterization of rainfall events

Pradeep V. Mandapaka,[1,2] Gabriele Villarini,[3] Bong-Chul Seo,[1] and Witold F. Krajewski[1]

Received 10 October 2009; revised 6 May 2010; accepted 11 May 2010; published 9 September 2010.

[1] Remotely sensed precipitation products, due to their large areal coverage and high resolution, have been widely used to provide information on the spatiotemporal structure of rainfall. However, it is well known that these precipitation products also suffer from large uncertainties that originate from various sources. In this study, we selected radar-rainfall (RR) data corresponding to 10 warm season events over a 256 × 256 km^2 domain with a data resolution of 4 × 4 km^2 in space and 1 h in time. We characterized their spatial structure using correlation function, power spectrum, and moment scaling function. We then employed a recently developed RR error model and rainfall generator to obtain an ensemble of probable rainfall fields that are consistent with the RR estimation error structure. We parameterized the spatial correlation functions with a two-parameter power exponential function, the Fourier spectra with a power law function, and the moment scaling functions with the universal multifractal model. The parameters estimated from the ensemble were compared with those obtained from the RR products to quantify the impact of radar-rainfall estimation errors on the spatial characterization of rainfall events. From the spatial correlation and power spectrum analyses, we observed that RR estimation uncertainties introduce spurious correlations with greater impact for the smaller scales. The RR errors also significantly bias the estimation of the moment scaling functions.

Citation: Mandapaka, P. V., G. Villarini, B.-C. Seo, and W. F. Krajewski (2010), Effect of radar-rainfall uncertainties on the spatial characterization of rainfall events, *J. Geophys. Res.*, *115*, D17110, doi:10.1029/2009JD013366.

1. Introduction

[2] Characterization of space-time variability of rainfall is paramount to many areas within the field of Earth sciences. This study focuses on the rainfall variability in space and the impact of radar-rainfall (RR) estimation uncertainties on the characterization of the spatial structure of rainfall. Several studies have characterized the spatial variability of rainfall by employing a variety of techniques ranging from correlation functions and variograms [e.g., *Sumner*, 1982; *Nicholson*, 1986; *Berndtsson*, 1988; *Bacchi and Kottegoda*, 1995; *Ricciardulli and Sardeshmukh*, 2002; *Krajewski et al.*, 2003; *Gebremichael and Krajewski*, 2004; *Ciach and Krajewski*, 2006; *Villarini et al.*, 2008] to multiscaling analysis tools such as moment scaling and structure functions [e.g., *Schertzer and Lovejoy*, 1987; *Tessier et al.*, 1993a; *Gupta and Waymire*, 1993; *Menabde et al.*, 1997; *Nykanen and Harris*, 2003; *Lovejoy and Schertzer*, 2006; *Gebremichael et al.*, 2008; *Lovejoy et al.*, 2008; *Morales and Poveda*, 2009; *Mandapaka et al.*, 2009b]. The spatial scales in the aforementioned studies ranged from a few meters to continental scales [e.g., *Lovejoy and Schertzer*, 2006; *Gebremichael et al.*, 2008; *Lovejoy et al.*, 2008; *Mandapaka et al.*, 2009b].

[3] While some early studies employed rain gauge networks to characterize the spatial variability of rainfall, use of remotely sensed data from radars and satellites has increased due to their wide spatial coverage. However, it is well known that rainfall products based on remotely sensed data contain random and systematic errors from various sources [e.g., *Bell et al.*, 1990; *Bell and Kundu*, 1996; *Smith et al.*, 1996; *Krajewski and Smith*, 2002; *McCollum et al.*, 2002; *Jordan et al.*, 2003; *Gebremichael et al.*, 2005; *Smith et al.*, 2006; *Ciach et al.*, 2007; *Germann et al.*, 2009; *Mandapaka et al.*, 2009a; *Villarini et al.*, 2009b; *Villarini and Krajewski*, 2010a; *Kirstetter et al.*, 2010]. Because of the lack of information on the rainfall estimation error structure, the majority of studies on the spatial characterization of rainfall have not accounted for the errors. Very few works [e.g., *Krajewski et al.*, 1996; *Villarini et al.*, 2007a, 2007b; *Villarini and Krajewski*, 2009a] have investigated the impact of rainfall estimation uncertainties on the spatial characterization of rainfall.

[4] *Krajewski et al.* [1996], in the first part of their study, processed the radar reflectivity data from the Darwin (Australia) radar using so-called "simple" and "complex"

[1]IIHR-Hydroscience and Engineering, University of Iowa, Iowa City, Iowa, USA.
[2]Now at MeteoSwiss, Locarno-Monti, CH-6605, Switzerland.
[3]Department of Civil and Environmental Engineering, Princeton University, Princeton, New Jersey, USA.

0148-0227/10/2009JD013366

algorithms and obtained rainfall fields at different scales (rain rates, hourly, and daily). They reported that the rainfall estimation algorithms have significant effect on the inferred statistics at hourly and daily scales. In the second part, they resorted to simulation experiment to better understand the effect of the RR estimation process on the inferred statistics. A "true" reference rainfall process (R) was simulated at a higher spatial resolution and converted into reflectivity fields (Z) by assuming a Z-R relation. Assuming these Z fields as the radar measured reflectivity fields, they simulated the radar estimation procedure by performing beam averaging, Z-R conversion, and polar-Cartesian grid conversion. In the process, they added random Gaussian (zero mean, 1 dBZ standard deviation) error fields resulting in an ensemble of RR fields. The statistics of R and RR fields were then compared to characterize the effect of errors induced during the radar observation process. They reported that the RR estimation (beam averaging, Z-R conversion, and polar-Cartesian grid conversion) has significant impact on the spatial characterization, leading to the underestimation of the coefficient of variation, overestimation of the spatial correlation distance, and underestimation of a certain random cascade parameter that characterizes the rainfall spatial intermittency. It is also worth mentioning that they employed three different statistical models to obtain the reference rainfall fields.

[5] *Villarini et al.* [2007a] analyzed the effect of systematic and random errors on the spatial multifractal properties of rainfall. The systematic effects that they investigated included the effect of zero-rain threshold, distance from the radar (range effect), and the parameters of the Z-R equation on the scaling behavior of the estimated statistical moments. They reported that the zero-rain threshold and distance from the radar have negligible effect on the estimated scaling functions. However, they also suggested that the range effect could be significant if a larger distance range were investigated in their study. The scaling of statistical moments was most sensitive to the exponent b in the Z-R relation. When the moments were plotted against the scale parameter in the log-log domain, they found that the regression line fitted to the moments was steeper for the lower values of the exponent b. To investigate the impact of random errors, they assumed that the RR fields were error free and convoluted them with uncorrelated and correlated lognormal error fields. They showed that the random errors would lead to the overestimation of the moment scaling functions. *Villarini et al.* [2007b] showed how nonmeteorological returns (ground clutter) in RR estimates could affect the estimation of the scaling function.

[6] The main limitation in the earlier two studies [*Krajewski et al.*, 1996; *Villarini et al.*, 2007a] was the arbitrary assumptions regarding the statistical structure of the RR error fields. *Villarini and Krajewski* [2009a] used a generator of probable true rainfall fields developed by *Villarini et al.* [2009a] (based on the data-driven RR error model in the work of *Ciach et al.* [2007]) and studied the combined effect of various sources of uncertainties in the RR estimation process on the generalized structure function of rainfall events. For a given RR field, they generated an ensemble of probable rainfall fields and showed that the RR estimation errors result in the overestimation of the structure functions for all of the 15 events considered in their study. Here we extend the analysis of *Villarini and Krajewski* [2009a] by investigating the effect of errors on the estimates of the spatial structure of rainfall fields. Specifically, we quantify the impact of RR errors on the spatial correlation function, power spectrum, and moment scaling function. For a given radar-rainfall event, we generate an ensemble of probable true rainfall events employing the error model by *Ciach et al.* [2007] and the rainfall generator by *Villarini et al.* [2009a]. We then compare the spatial dependence estimates for the RR product with those of probable rainfall events to quantify the effect of the RR estimation errors on the spatial characterization of rainfall events.

[7] This paper is organized as follows: In section 2, we describe the RR data used in this study. A short description of the RR error model and the probable rainfall generator is presented in section 3. Section 4 briefly describes the analysis tools employed to characterize the rainfall events. The results are discussed in section 5, followed by conclusions in section 6.

2. Radar-Rainfall Data

[8] Customized high-resolution RR data with a spatial resolution of 1×1 km^2 and a temporal resolution of 15 min were obtained from the Pseudo-Precipitation Processing System (PPPS) and Hi-Fi algorithms of the Hydro-NEXRAD system of data distribution [e.g., *Krajewski et al.*, 2010] at the University of Iowa. *Krajewski et al.* [2010] provide an overview of the Hydro-NEXRAD system and the algorithms used to create the RR products. Radar-rainfall products obtained from the Hydro-NEXRAD system have been used in previous studies published in the literature [e.g., *Ntelekos et al.*, 2008, 2009; *Villarini and Krajewski*, 2010b, *Villarini et al.*, 2010]. Here we give a brief description of the PPPS and Hi-Fi algorithms.

[9] PPPS is the Hydro-NEXRAD implementation of the National Weather Service's (NWS) Precipitation Processing System algorithm [e.g., *Fulton et al.*, 1998] that enables us to obtain PPPS radar-rainfall products at higher spatial and temporal resolutions (1×1 km^2 and 15 min) than the operational products. We refer to it as Pseudo-PPS since, despite using the same logic and major algorithmic steps, it does not reproduce exactly the official NWS products that account for predefined site-specific information such as clutter and terrain occultation maps.

[10] In the Hi-Fi products, corrections are performed to mitigate the errors due to anomalous propagation, range effect, and storm advection. The procedure for constructing the hybrid scan is different for the PPPS and Hi-Fi products. While PPPS takes reflectivity values from the angle that corresponds to 1.0 km above radar altitude, Hi-Fi uses kernel smoothing to alleviate a discontinuity problem in the rainfall maps and to suppress no-rain echoes around the radar [*Seo et al.*, 2009]. The zero-rainfall threshold for the reflectivity values is also different for the PPPS and Hi-Fi rainfall products. It is equal to 18 dBZ for the former and 10 dBZ for the latter. The factors mentioned above may result in differences in rainfall amounts at the level of final products.

[11] We selected 10 rainfall events measured by Weather Surveillance Radar-88 Doppler (WSR-88D) [e.g., *Crum*

Table 1. List of the Selected Rainfall Events Indicating the Beginning, End, Duration, and the Overall Accumulation[a]

Storm ID	Begin mm/dd/yyyy	End mm/dd/yyyy	N (h)	Accumulation (mm)	
				PPPS	Hi-Fi
KICT-01	06/30/2004 15:15	07/03/2004 03:00	60	32.58	30.92
KICT-02	07/26/2005 02:15	07/27/2005 10:00	32	7.97	7.13
KICT-03	08/12/2005 15:15	08/14/2005 12:00	45	36.89	36.78
KICT-04	08/24/2005 02:15	08/25/2005 21:00	43	58.36	53.95
KICT-05	06/21/2006 20:15	06/22/2006 16:00	20	22.45	21.31
KICT-06	07/26/2006 20:15	07/27/2006 19:00	23	11.31	11.30
KICT-07	05/05/2007 20:15	05/07/2007 11:00	39	94.32	86.18
KICT-08	06/26/2007 12:15	07/01/2007 00:00	108	84.37	80.02
KICT-09	07/27/2007 15:15	07/31/2007 17:00	98	26.68	26.10
KICT-10	05/07/2008 00:15	05/08/2008 03:00	27	45.11	42.42

[a]The accumulation value is shown for the rainfall events obtained from Pseudo-PPS (PPPS) and Hi-Fi algorithms. The size of the domain is 256 × 256 km^2 with the KICT radar at its center. The spatial resolution of the data is 4 km.

and Alberty, 1993; *Klazura and Imy*, 1993] radar in Wichita, Kansas (KICT), and obtained the high-resolution rainfall products using the aforementioned algorithms for a square domain of 256 × 256 km^2 with the radar at its center. Table 1 lists the time of occurrence, duration, and the storm total accumulation for the PPPS and Hi-Fi products of the 10 rainfall events. We have selected only warm season (May–August) events to avoid seasonal effects. The events KICT-05 and KICT-06 are shorter duration events lasting for less than a day, while KICT-08 and KICT-09 are longer events lasting for more than 4 days (Table 1). The storm total varies from about 7 to 90 mm. Table 1 illustrates that the storm accumulation for the products based on the two algorithms does not vary greatly.

3. Radar-Rainfall Error Model

[12] *Ciach et al.* [2007] proposed a product error–driven (PED) model for RR estimation errors, in which the relation between true areal rainfall and radar-rainfall was described by two multiplicative components: a systematic distortion function and a stochastic component. Both components were conditioned on the RR values. While the systematic function accounts for biases conditional on the RR values, the stochastic component accounts for the remaining random errors. The results in the work of *Ciach et al.* [2007] were based on a large sample (6 years) of hourly accumulation fields (Digital Precipitation Arrays; *Fulton et al.*, 1998) from the Oklahoma City radar, averaged over 4 km pixels, and generated with the Precipitation Processing System (PPS) [*Fulton et al.*, 1998]. Radar-rainfall estimates were complemented with rain gauge measurements, which were used as an approximation of the true ground rainfall. To account for seasonality and range effects, the parameters of the model were estimated for three seasons (cold, warm, and hot) and five spatial zones at different distances from the radar location. *Ciach et al.* [2007] showed how the systematic distortion function could be approximated by a power law function, while the random component was parameterized by a Gaussian distribution, with mean equal to 1, standard deviation that was a hyperbolic function of rainfall, and with significant correlation both in space and time. The error model by *Ciach et al.* [2007] was then used by *Villarini et al.* [2009a] to develop a generator of probable true rainfall fields conditioned on hourly radar-rainfall maps. As discussed in the work of *Villarini et al.* [2009a], the generator accounts for the conditional and unconditional biases, nonstationarity in variance, and spatial correlation of the random component but not for the temporal dependencies.

[13] In this study, we assumed that the parameters of the systematic and random components for the Oklahoma City radar [*Ciach et al.*, 2007] could be used to describe the uncertainties in the RR products generated from the KICT radar in Wichita, Kansas. There is no guarantee that the parameters for the Oklahoma City radar are valid for the KICT radar, even though there is evidence that the overall model structure should be valid [*Villarini and Krajewski*, 2009b]. The transferability of the results in the work of *Ciach et al.* [2007] to other radars should be investigated in future studies. Moreover, the differences in the parameters of the error model obtained using PPS or Pseudo-PPS appear not to be significant [*Villarini and Krajewski*, 2010b]. The probable rainfall fields were obtained as follows: (1) the given RR field was first corrected for the overall (unconditional) bias; (2) for each pixel, the corresponding RR estimate was then corrected for conditional bias (bias function of the RR estimate); (3) an ensemble of spatially correlated Gaussian fields with a unit mean and standard deviation conditional on RR field were then generated using the Cholesky decomposition method; (4) the correlated Gaussian ensemble was then multiplied with the bias corrected RR fields (steps 1 and 2) to obtain an ensemble of probable rainfall fields. The parameters required for the steps 1–3 were obtained from the work of *Ciach et al.* [2007].

[14] We performed our analyses for the Pseudo-PPS products aggregated to 4 × 4 km^2 and hourly scales since these are the scales used in the work of *Ciach et al.* [2007]. The time series of hourly accumulations for the 10 events are shown in Figure 1. It is possible to repeat the analysis of *Ciach et al.* [2007] for smaller space-time scales and use those parameters. There are two main reasons why we did not perform such an analysis. (1) Extending the PED model of *Ciach et al.* [2007] to smaller temporal and spatial scales represents a significant effort that is beyond the scope of the present study. It would require generating 6 years worth of rainfall products as well as an investigation of the effect of the rain gauge representativeness error (*Ciach et al.* [2007] neglect the subgrid rainfall variability effects). (2)

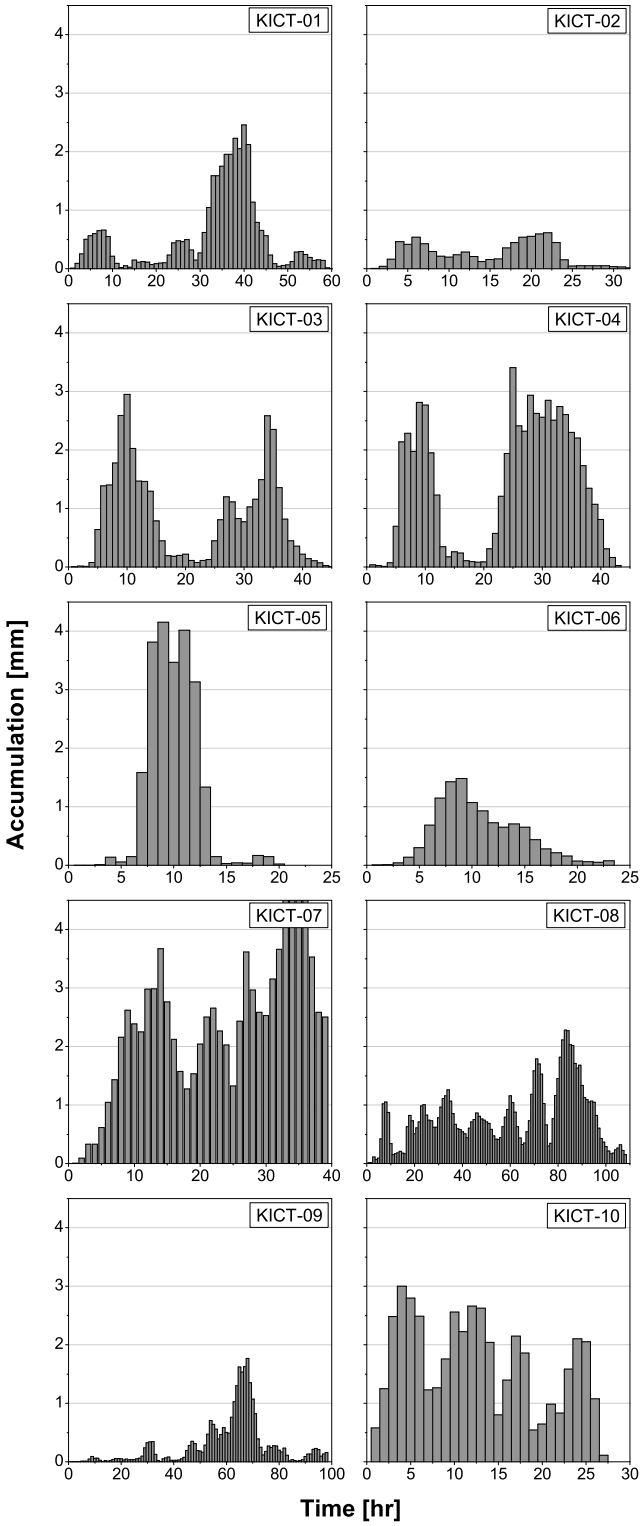

Figure 1. Time series of hourly accumulations for the selected storms. The radar-rainfall fields are generated using the Pseudo-PPS algorithms. The storm IDs are indicated on each panel. The maximum accumulation for KICT-07 is 5.5 mm. However, we truncated the axis at 4.5 mm for clarity.

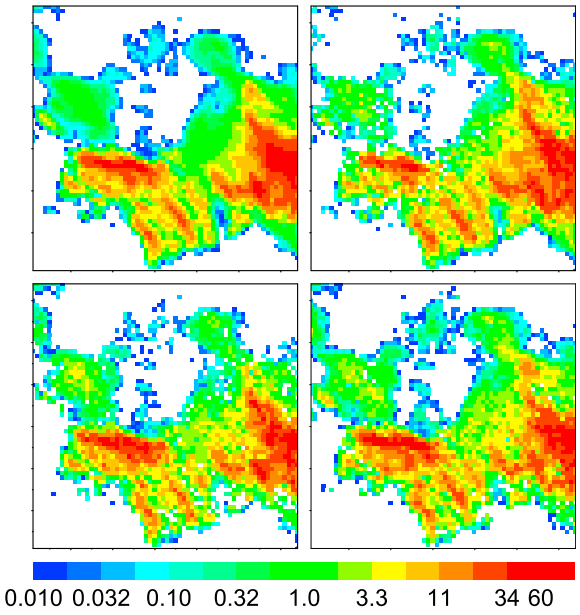

Figure 2. Radar-rainfall hourly accumulation field (in mm) from the storm KICT-04 (top left) and the sample realizations generated using the model described in the work of *Villarini et al.* [2009a].

The PED generator of *Villarini et al.* [2009a] generates spatially correlated Gaussian fields based on the Cholesky decomposition of the covariance matrix. For the same domain size (256 km) and higher resolution, the size of the covariance matrix is much larger and it is computationally intensive (requiring floating point operations ~ $O(n^5)$ for a grid size of $n \times n$) to solve the matrix using the Cholesky technique. Notwithstanding the fact that the parameters of the error model are available for the hourly scale and 4 km pixels, our choice of 4×4 km^2 is also a trade-off between computational requirements and the spatial variability. Figure 2 shows Pseudo-PPS hourly RR field from the event KICT-04, and three sample realizations were generated using *Villarini et al.* [2009a].

4. Analysis Tools

[15] This section briefly describes the analysis techniques as applied to the selected rainfall events. We start with the description of how the spatial correlation functions were estimated for each rainfall event and then proceed to an estimation of scaling analysis tools such as the power spectrum and the moment scaling function. For all of the analysis tools, we assumed that the RR accumulation fields are temporally independent. We checked the validity of this assumption by estimating the temporal correlations for the spatial scales ranging from 4 to 128 km. For the smaller spatial scales, the "*e*-folding" time (defined as the time at which the correlation drops to 1/*e*) ranged from ~1 to ~3 h (figure not shown). For 128 km spatial scale, the *e*-folding time varied from ~2 to ~6 h (figure not shown). However, it should be noted that the estimation of these correlations suffers from the sampling issue, particularly for larger spatial scales of 128 km.

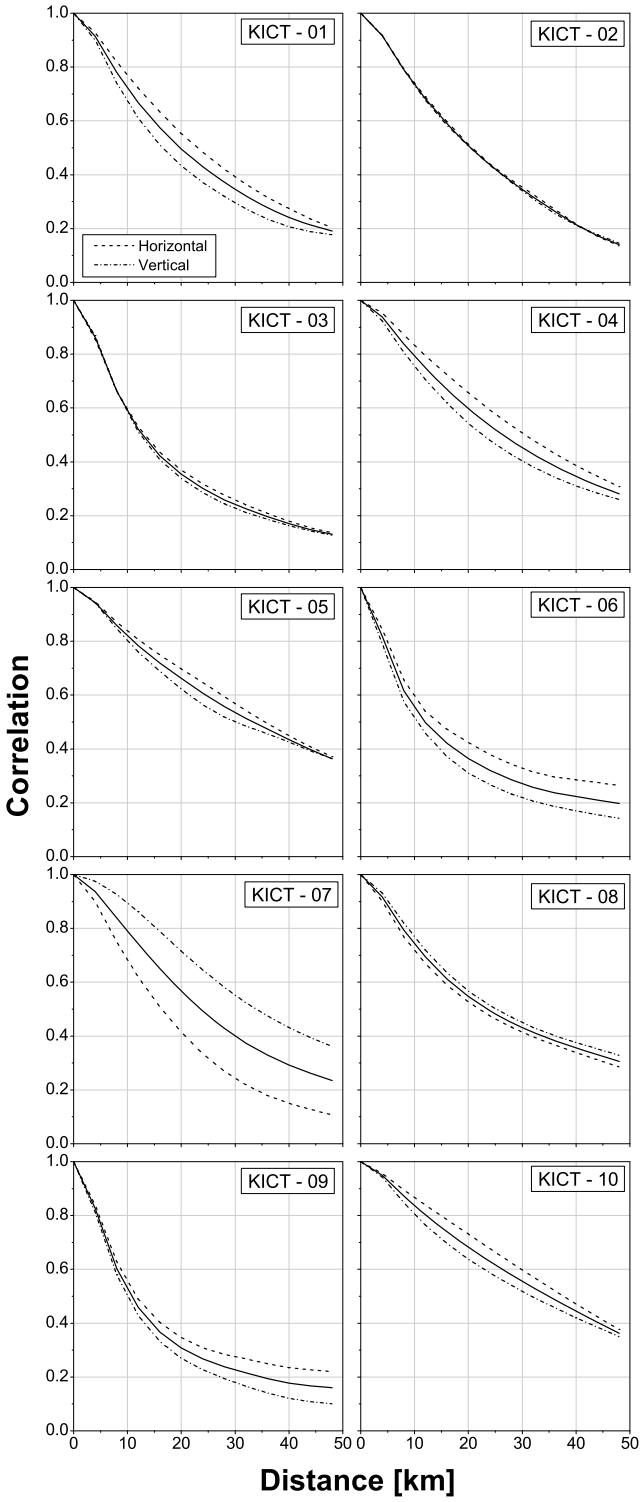

Figure 3. Spatial correlation functions estimated in the horizontal and vertical directions. The solid dark line indicates the correlations estimated assuming isotropy.

4.1. Spatial Correlation Function

[16] The correlation is a normalized measure of the linear association between two random vectors. We used the Pearson's product moment estimator to obtain the correlation of the process $\{Z(u): u \in R^2\}$ for all u_i and u_j in an $n \times n$ grid such that $\{u_i - u_j = d;\ i,j = 1,2,\ldots,n^2\}$,

$$\rho(d) = \frac{\langle Z(u_i)Z(u_j)\rangle - \langle Z(u_i)\rangle\langle Z(u_j)\rangle}{\sqrt{\langle Z(u_i)^2\rangle - \langle Z(u_i)\rangle^2} \times \sqrt{\langle Z(u_j)^2\rangle - \langle Z(u_j)\rangle^2}}, \quad (1)$$

where $\langle\cdot\rangle$ represents the expectation operator and $\rho(d)$ is the correlation for a distance lag d. For each storm, we estimated the spatial correlation for horizontal (X) and vertical (Y) directions. Figure 3 compares X and Y correlations with those of isotropic scenario. The difference in directional correlations was found to be negligible for the storms KICT-02, KICT-03, and KICT-08, while KICT-07 displayed highest sensitivity (Figure 3). However, we assumed isotropy for all the storms including KICT-07 for the sake of consistency. Since this assumption is applied to the probable rainfall fields as well, we believe that it will not have a major impact on the main goal of this study, which is to characterize the effect of RR errors on the estimated correlations. It should also be noted that checking correlations in just two directions is not a sufficient condition to establish isotropy.

[17] Assuming isotropy in space and independence in time, the averages in equation (1) were estimated by pooling together the pixel values that correspond to the distance lag d in all of the rainfall fields. In this study, d varied from 0 to approximately 48 km. The estimated correlations, when plotted against the distance lag, represent the spatial correlation function. If the correlation drops rapidly with distance, then the process is considered highly variable in space. The correlation functions were parameterized by fitting a two-parameter power exponential function of the form,

$$\rho(d) = \exp[-(d/\theta_1)^{\theta_2}] \quad \theta_1 > 0,\ 0 \le \theta_2 \le 2\,, \quad (2)$$

using the Levenberg-Marquardt algorithm. The parameter θ_1 in equation (2) is the correlation distance, defined as the distance for which the correlation coefficient is equal to $1/e$, and θ_2 is the shape parameter that controls the correlation function near the origin. We selected this correlation model because it is widely used to model such spatial processes as hydraulic conductivity and rainfall [e.g., *Bacchi and Kottegoda*, 1995; *Gebremichael and Krajewski*, 2004; *Stauffer*, 2005; *Ciach and Krajewski*, 2006; *Villarini et al.*, 2008].

4.2. Power Spectrum

[18] A physical process is said to be scale invariant or scaling if large-scale and small-scale structures are related by a scale-changing operation that involves only the scale ratio and an exponent [e.g., *Schertzer and Lovejoy*, 1987]. In addition to understanding the rainfall process across multiple scales, other attractive features of the scaling framework are that parsimonious models can be developed to generate synthetic rainfall fields at a given resolution and statistical downscaling techniques can be developed to obtain rainfall fields at much higher resolution.

[19] The Fourier power spectrum is one of the most widely used tools to detect the presence of scale invariance

in rainfall. The power spectrum of the rainfall event was obtained as follows:

[20] 1. Each rainfall accumulation field is Fourier transformed, and the amplitudes are modulus squared to obtain the 2-D power spectrum.

[21] 2. The 2-D power spectrum, which is conjugate symmetric, is folded about the Nyquist frequency.

[22] 3. Assuming isotropy, the folded spectrum is radially averaged about the corner.

[23] A process is said to be scale invariant if the power spectrum displays log-log linearity (power law) within a finite range of frequencies. If $E(f)$ is the power for the frequency f, then the scale-invariant field will have a power spectrum of the form

$$E(f) = f^{-\beta}, \tag{3}$$

where β is the slope of the spectrum in the log-log domain. The power spectrum slope is an indicator of the spatial organization of the field. The higher the value of β, the smoother and more organized the rainfall field [e.g., *Purdy et al.*, 2001; *Nykanen and Harris*, 2003]. It should be noted that for the fields with a fixed resolution, the power spectrum is distributed in uniform frequency (or wave number) bins. When such a spectrum is plotted in a double logarithmic plot, most of the spectrum is concentrated towards higher frequencies. To avoid excess weighting on the higher frequencies, we estimated β by performing ordinary least squares regression on the octave binned power spectrum [e.g., *Harris et al.*, 1997] in the double-logarithmic domain. The log-log linearity was checked based on the R^2 value in linear regression.

4.3. Spatial Moment Scaling Analysis

[24] The next tool we used in this study is the moment scaling analysis to investigate the presence of multifractality. For a multifractal process, it has been shown [e.g., *Menabde et al.*, 1997] that the spectral slope β is always less than the dimension (D) of the field. If $\beta > D$, which is often the case with geophysical phenomena including rainfall, moment scaling analysis has to be performed on either the fractionally differentiated field [e.g., *Schertzer and Lovejoy*, 1987; *Nykanen and Harris*, 2003] or on the small-scale fluctuations (gradient) of the original field [e.g., *Tessier et al.*, 1993a; *Menabde et al.*, 1997].

[25] In this study, we adopted the latter approach and obtained small-scale fluctuations as the difference between the value at the given pixel and the mean of the four nearest neighbors (three for edge pixels and two for the ones on the corner). For each rainfall event, the gradient fields of resolution r (= 4 km) and size L (= 256 km) were then averaged over a range of scales $l(n)$. The value of n varies from 0 to 6, with $l(0)$ equal to 4 km and $l(6)$ equal to 256 km. The averaged fields are referred to as φ_λ, where λ is the ratio of the size of the field L to the averaging scale $l(n)$. We estimated the correlations in time for different spatial scales to check the temporal structure of hourly fluctuation fields. The e-folding time for smaller spatial scales ranged from ~1 to ~3 h while it ranged ~2 to ~5 h for 128 km aggregations. Therefore, assuming that the fluctuation fields within the rainfall event were time independent, the average values in the φ_λ fields at all of the time steps were pooled together, and the trace moments $M_q(\lambda)$ of various moment orders q were estimated for each scale ratio λ. The higher the value of λ, the larger the sample size available to estimate the moments.

[26] The gradient field is multifractal if there is a scaling relationship of the form

$$M_q(\lambda) = \langle \varphi_\lambda(x,y)^q \rangle \sim \lambda^{K(q)}, \tag{4}$$

where $K(q)$ (the slope of $M_q(\lambda)$ versus λ in the log-log domain) is a nonlinear function of the moment order q. Theoretically, $K(q)$ is required for q values ranging from 0 to ∞ to fully characterize the multifractality in the rainfall fluctuation fields. However, *Tessier et al.* [1993a] proposed a universal multifractal (UM) model for $K(q)$ based on multiplicative cascades consisting of parameters α and C_1,

$$K(q) = \frac{C_1}{\alpha - 1}(q^\alpha - q) \quad 0 \le \alpha < 1 \ \text{ and } \ 1 < \alpha \le 2, \tag{5}$$

$$K(q) = C_1 q \log q \qquad \alpha = 1. \tag{6}$$

The parameter α is the Levy-stable (or multifractality) index that characterizes the spikiness and indicates the probability distribution from which the weights are generated in the cascading process. The case $0 < \alpha < 2$ ($\alpha \neq 1$) corresponds to log(Levy) multifractals, and if $\alpha = 1$ the multifractal process is log(Cauchy) [e.g., *Tessier et al.*, 1993a]. The case with $\alpha = 2$ corresponds to lognormal multifractals. C_1 is the intermittency parameter that characterizes the sparseness of the mean. It should be noted that the above model (equations (5) and (6)) is for the conservative cascades for which $\beta < D$. However, rainfall fields often display a nonconservative, multiaffine nature with a power spectrum slope greater than the dimension of the process. The degree of nonconservation is quantified in terms of the Hurst exponent H, estimated as

$$H = \frac{[\beta - D + K(2)]}{2}, \tag{7}$$

where $K(2)$ is the scaling exponent corresponding to the second moment order. The Hurst exponent is also an indicator of the smoothness of the field [e.g., *Harris et al.*, 2003].

[27] In this study, the parameters C_1 and α were obtained using the double trace moments (DTM) technique [e.g., *Tessier et al.*, 1993a]. In the DTM technique, we take various powers η of the rainfall fluctuations at their highest resolution, average the powered fluctuations to various spatial scales with scale ratio λ, and estimate the statistical moments (referred to as double trace moments) of various orders q,

$$M_{\eta,q}(\lambda) = \left\langle (\varphi^\eta(x,y))_\lambda^q \right\rangle. \tag{8}$$

In the case of universality, the double trace moments will depend on the scale ratio as [e.g., *Tessier et al.*, 1993a],

$$M_{\eta,q}(\lambda) \sim \lambda^{K(q,\eta)} \tag{9}$$

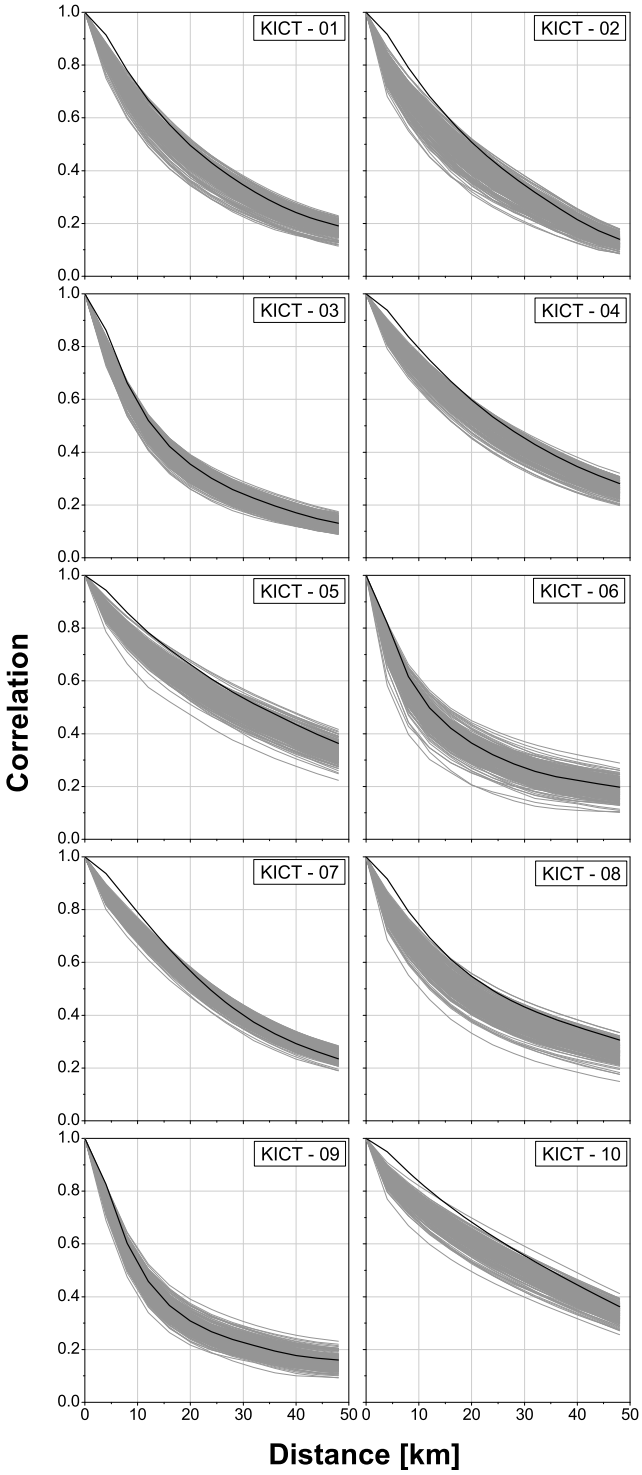

Figure 4. Effect of radar-rainfall errors on the spatial correlation function. The solid dark line represents the correlation function obtained for the Pseudo-PPS rainfall product, whereas the gray lines are the correlation functions for the ensemble of probable rainfall fields generated using the model described in the work of *Villarini et al.* [2009a].

and

$$K(q,\eta) = \eta^{\alpha} \cdot K(q). \tag{10}$$

Therefore, α is the slope of $K(q,\eta)$ versus η in a double logarithmic plot for a fixed q. The value of C_1 can be obtained by plugging α in equation (5) for a fixed q. For a detailed description of the DTM technique, the reader is referred to *Tessier et al.* [1993a]. Several studies have applied the UM model over the last 15 years to describe a variety of geophysical phenomena such as wind and atmospheric temperature [e.g., *Schmitt et al.*, 1994, 1996; *Lazarev et al.*, 1994], rain and clouds [*Tessier et al.*, 1993a; *Hubert et al.*, 1993; *Naud et al.*, 1996; *Marsan et al.*, 1996], ocean surface [*Tessier et al.*, 1993b], hydraulic conductivity [e.g., *Liu and Molz*, 1997], and topography [e.g., *Lavallee et al.*, 1993; *Tchiguirinskaia et al.*, 2000; *Gagnon et al.*, 2006].

5. Results and Discussion

[28] First, we compared the aforementioned spatial characterization estimates for the PPPS and Hi-Fi radar-rainfall products of each event in Table 1 to see if corrections involved during the generation of Hi-Fi products altered the estimated spatial structure. Then, we generated an ensemble of 200 probable true events using the rainfall generator (section 3) and conditioned on the PPPS storm data (for each event). We compared the estimates for the PPPS product with those of probable rainfall events to assess the impact that the rainfall estimation errors in the PPPS product had on the spatial characterization of rainfall events.

5.1. Effect on Spatial Correlation Function

[29] The spatial correlations were estimated for the radar-rainfall data using Pearson's product moment estimator (equation (1)). The dark solid line in Figure 4 represents the correlation estimates plotted against the distance lag for the rainfall products obtained using the Pseudo-PPS algorithm. We noticed that the correlation estimates for PPPS and Hi-Fi algorithms were quite close, meaning that the spatial correlation structure was not sensitive to the corrections performed during the creation of Hi-Fi rainfall products. For the sake of clarity, we did not plot the corresponding estimates for the Hi-Fi product. The correlation estimates were fitted using the two-parameter exponential function (equation (2)), and the parameters (correlation distance and shape parameter) are given in Table 2 for both radar-rainfall algorithms. The correlation distance varied from a minimum value of around 18 km for the storm KICT-09 to a maximum value of about 48 km for the storm KICT-10 (Table 2). The shape parameter ranged between 0.74 and 1.20. If the shape parameter is smaller than 1.0, the small-scale correlations drop faster than exponential, while if it is greater than 1.0, the correlations decay at a much slower rate than the corresponding exponential one. From the values of correlation distances and shape parameters, we can infer that the storms KICT-03, KICT-06, and KICT-09 are more variable than the others. Similarly, the storms KICT-04, KICT-05, and KICT-10 are smoother than the other events considered.

[30] The gray lines in Figure 4 represent the spatial correlation functions estimated from each of the 200 probable rainfall events. From Figure 4, it can be seen that the effect

Table 2. Parameters of the Spatial Correlation Function Estimated From the Radar-Rainfall Data Obtained From Pseudo-PPS (PPPS) and Hi-Fi Algorithms[a]

	Correlation Distance (km)					Shape Factor				
			Probable Rainfall					Probable Rainfall		
Storm ID	PPPS	Hi-Fi	$Q_{0.05}$	Mean	$Q_{0.95}$	PPPS	Hi-Fi	$Q_{0.05}$	Mean	$Q_{0.95}$
KICT-01	28.61	28.23	20.81	25.49	29.62	1.07	1.07	0.83	0.90	0.96
KICT-02	27.90	28.20	18.76	23.52	27.95	1.18	1.19	0.79	0.90	1.01
KICT-03	20.44	20.39	16.00	18.93	21.78	0.93	0.92	0.78	0.82	0.87
KICT-04	37.59	36.53	29.66	34.54	39.54	1.09	1.10	0.83	0.89	0.94
KICT-05	47.24	46.40	35.84	43.84	52.16	1.04	1.06	0.77	0.84	0.93
KICT-06	21.55	22.71	14.57	19.66	25.13	0.74	0.75	0.58	0.65	0.72
KICT-07	33.25	32.60	29.45	32.90	36.10	1.16	1.16	0.86	0.93	0.99
KICT-08	37.53	38.02	24.09	30.84	38.03	0.90	0.91	0.66	0.71	0.77
KICT-09	18.39	18.10	13.93	17.38	21.10	0.80	0.78	0.70	0.73	0.77
KICT-10	48.03	50.73	38.27	46.12	52.21	1.11	1.13	0.74	0.82	0.90

[a]The table also shows the mean and 5th and 95th percentiles of the corresponding parameters for the probable rainfall fields. All of the parameters are estimated for hourly accumulations averaged over a 4 km grid.

of RR errors on the correlation estimates varies with each storm. The bias is clearly evident for storms KICT-05 and KICT-10, whereas the bias is not noticeable for the storms KICT-06 and KICT-09 (Figure 4). We estimated the correlation distance and shape parameter (θ_1 and θ_2 in equation (2)) for each of the 200 correlation functions. Table 2 lists the average and 5th and 95th percentiles of the parameters estimated from the ensemble of probable rainfall events. Hereafter, we compare the parameters of the ensemble with those of the PPPS product, as the ensemble rainfall events were generated conditional on the PPPS product.

[31] The correlation distance for the PPPS product is greater than the average θ_1 from the ensemble rainfall events for all the storms (Table 2). Nonetheless, θ_1 of the PPPS product is always within the 90% confidence interval obtained from the probable rainfall events (Table 2). Therefore, there is not enough statistical evidence (at the 10% significance) to say that the correlation distance of the PPPS product is overestimated. The impact of RR errors is more pronounced for the shape parameter. The estimates of the shape parameter for the PPPS product are always greater than the average shape parameter from the probable rainfall fields (Table 2). Moreover, they are always larger than the 95th percentile. From the above analysis, it can be said that the RR estimation errors significantly affect the estimation of spatial correlations at smaller scales.

5.2. Effect on Power Spectrum

[32] Although the spatial correlation function provides information on the variability of the rainfall fields, it does not tell us how the small-scale and large-scale structures in rainfall interact with each other. Several studies in the literature focused on the relation between the multiscale statistical properties and the meteorological features of the storm [e.g., *Perica and Foufoula-Georgiou*, 1996; *Purdy et al.*, 2001; *Nykanen and Harris*, 2003; *Nykanen*, 2008]. We estimated the power spectrum slope (β) for each accumulation field using the algorithm discussed in section 4.2 and followed its evolution (Figure 5). For all the storms, an increasing spectral slope at the beginning stages of the storm can be noticed followed by a stationary region and a decreasing β (Figure 5). The falling limb was not evident for KICT-07, as the data pertaining to the decaying part of the storm was not available (see Figure 1). However, for most parts of the storms, the behavior of β is stationary. Therefore, we did not attempt to relate the meteorological features of a storm to its statistical characteristics. We averaged the individual spectra estimated for each accumulation field and estimated one power spectrum slope for each storm. The corresponding β is shown in Figure 5 with a dotted line and in Table 3. Similar to the correlation estimates, the corrections performed in the Hi-Fi rainfall products had negligible effect on the power spectrum slope (Table 3).

[33] Figure 6 (dark lines) shows the average power spectrum for the rainfall products generated using the PPPS algorithm. Except for the slight departure towards the lower wave numbers (e.g., dark line for event KICT-02 in Figure 6), caused mainly by sampling effects, the power spectrum displayed log-log linearity for most of the domain. The slope β was then estimated for the region between the spatial scales of 32 km (wave number ~ 8) and 8 km (wave number ~ 32) using the octave binning technique [e.g., *Harris et al.*, 1997]. Since linear regression was performed on the octave-binned spectrum, the sampling issue does not significantly affect the estimation of the slope β. The R^2 value in the linear regression was always greater than 0.97, confirming log-log linearity of the spectrum. The spectral exponents for all of the events are listed in Table 2. The values of β ranged from 2.05 to 2.88, with lower values for the storms KICT-06 and KICT-09 and higher values for KICT-04 and KICT-10. The highest value of β for KICT-10 indicates a smoother and more organized rainfall event, which is in agreement with the results from the correlation analysis that reported high values of correlation distance and shape parameter for that particular event.

[34] The power spectra estimated for an ensemble of probable rainfall fields (gray lines in Figure 6) also displayed log-log linearity for most of the frequency domain. Comparing the spectrum obtained from PPPS products with those of the probable rainfall events, we notice that the errors have a larger impact towards higher frequencies or smaller scales (Figure 6). The effect of errors is to smooth the rainfall fields at small scales, thereby decreasing the contribution of higher frequencies and increasing the value

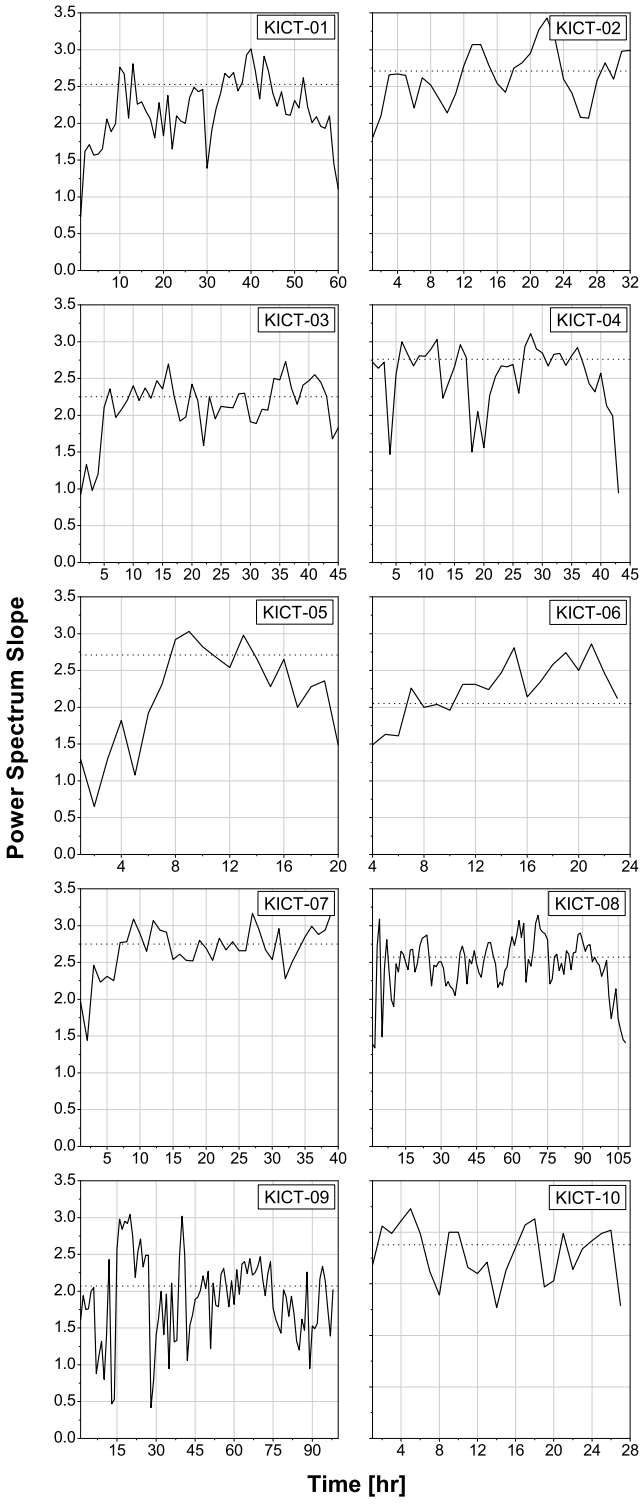

Figure 5. Temporal evolution of the slope of the power spectrum estimated for the Pseudo-PPS products of 10 rainfall events in Table 1. The dotted line in each panel represents the power spectrum slope estimated by combining all the accumulation fields in time.

of β. The β value for the PPPS RR product was greater than the average β from the probable rainfall events for all of the storms (Table 3). Except for the storms KICT-06 and KICT-09, the β value falls outside the 90% confidence interval obtained for the probable rainfall events (Table 3). The events KICT-06 and KICT-09 also happen to be the most variable of all the events considered in the study (Tables 2 and 3). Even in the correlation analysis, the bias in shape parameter is smaller for storms KICT-06 and KICT-09. With the exception of these two storms, the RR errors result in the overestimation of the power spectrum slope (the value is larger than the 95th percentile). The small-scale smoothing effect of the RR errors is consistent with the results from the correlation analysis.

5.3. Effect on Moment Scaling Function

[35] The value of β from the power spectrum analysis was always greater than the dimension of the field for all the rainfall events. Therefore, as mentioned in section 4.3, moment scaling analysis has to be performed on the gradient of rainfall fields. We obtained the gradient fields following the methodology proposed by *Menabde et al.* [1997], which was briefly described in section 4.3. The gradient fields were averaged to various spatial scales, and the trace moments (equation (4)) were estimated for moment orders ranging from 0.1 to 4.0. The trace moments of various orders estimated for all the rainfall events are shown in Figure 7. One could obtain the error bars for trace moments at each spatial scale by a resampling technique, but the sample size to estimate the moments would be smaller in each iteration and the corresponding error bars may not give the correct picture of the sampling effect. Therefore, we chose to not show error bars for the estimated moments.

[36] We estimated the slopes (scaling exponents) by first considering all seven scales (λ = 1, 2, 4, 8, 16, 32, and 64) in the regression analysis and then by excluding the larger scales of λ = 1 and λ = 1, 2, respectively. Figure 8 illustrates the effect of sampling on the estimation of moment scaling exponents: the slopes are in general steeper, when larger scales are considered in the regression. Therefore, to minimize the effect of sampling on the estimation of scaling exponents, we excluded the larger scales of λ = 1, 2 in our study. The corresponding fitted regression lines are shown in Figure 7. The R^2 value in the regression was always greater

Table 3. The Power Spectrum Slope Estimated Using Ordinary Least Squares Regression for the Radar-Rainfall Data Obtained From Pseudo-PPS (PPPS) and Hi-Fi Algorithms[a]

	Power Spectrum Exponent β				
			Probable Rainfall		
Storm ID	PPPS	Hi-Fi	$Q_{0.05}$	Mean	$Q_{0.95}$
KICT-01	2.53	2.53	2.15	2.29	2.41
KICT-02	2.71	2.73	2.17	2.35	2.51
KICT-03	2.25	2.25	2.01	2.11	2.21
KICT-04	2.76	2.77	2.33	2.46	2.57
KICT-05	2.71	2.72	2.30	2.44	2.58
KICT-06	2.05	2.10	1.80	1.94	2.09
KICT-07	2.75	2.75	2.37	2.48	2.58
KICT-08	2.57	2.60	2.10	2.25	2.40
KICT-09	2.07	2.05	1.86	1.99	2.09
KICT-10	2.88	2.94	2.36	2.49	2.61

[a]The table also shows the mean and 5th and 95th percentiles of the corresponding parameters for the probable rainfall fields. All of the parameters are estimated for hourly accumulations averaged over a 4 km grid.

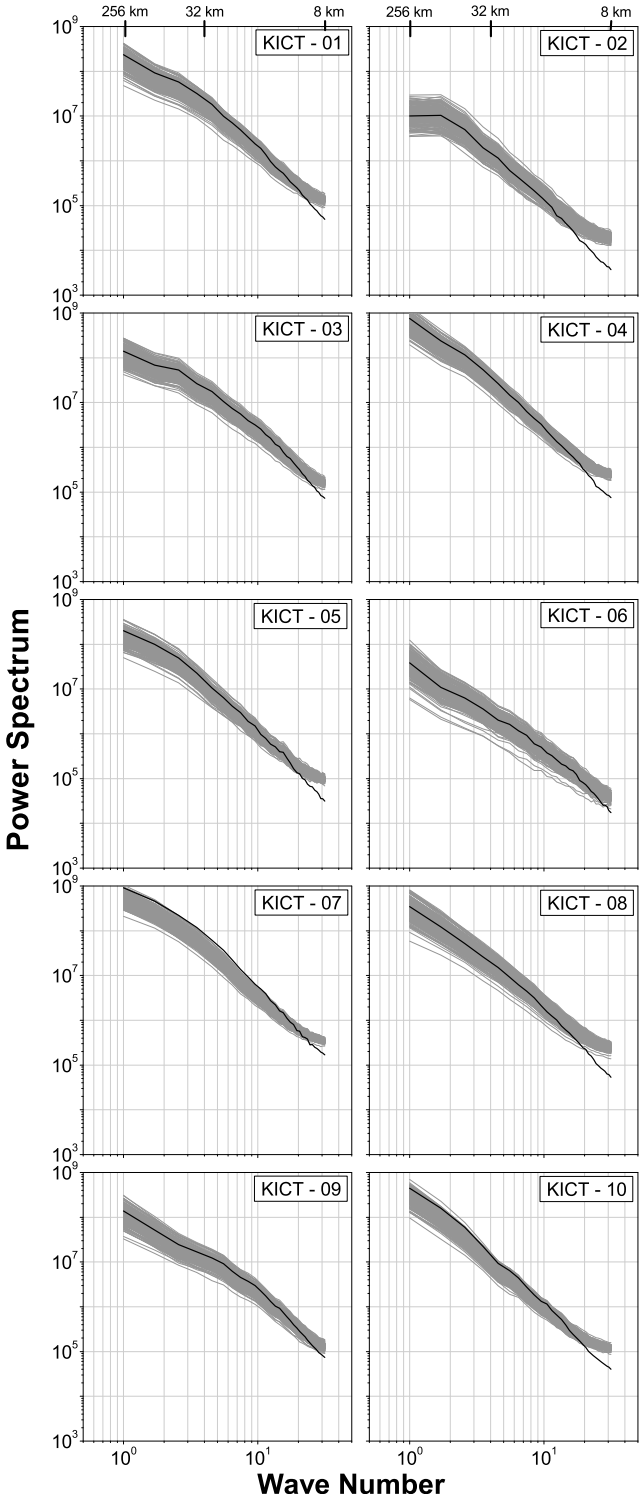

Figure 6. Same as Figure 4, but for the power spectrum.

than 0.98, confirming the log-log linearity of moments. For all the rainfall events, the slopes varied nonlinearly with the moment order, indicating that the rainfall gradients were multiscaling (Figure 8). We obtained the moment scaling exponents for all of the 200 probable rainfall events and compared them with those of PPPS product in Figure 9.

The effect of RR errors varied for each storm, with noticeable bias for the storms KICT-01, KICT-08, and KICT-10 and small bias for the storms KICT-02, KICT-04, and KICT-07 (Figure 9).

[37] We parameterized the moment scaling exponents with the universal multifractal model (equations (5) and (6)) using the double trace moment technique described in

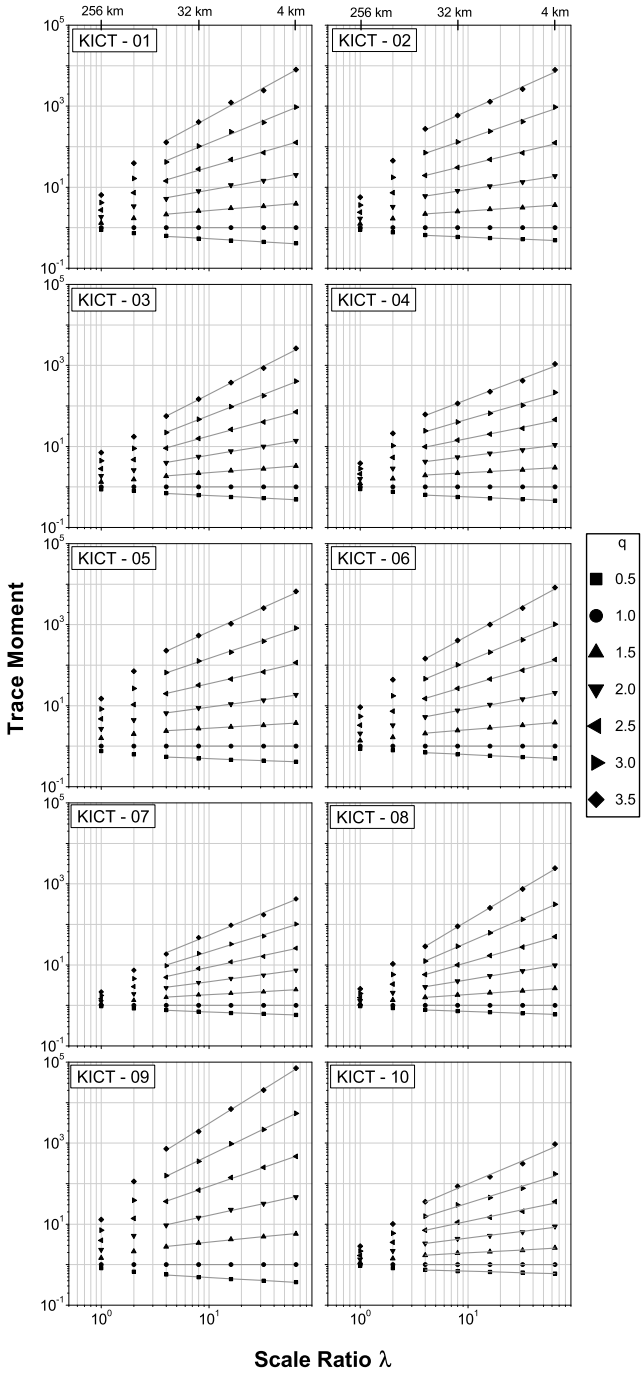

Figure 7. Scaling of trace moments of different moment orders q with the scale ratio λ, for the Pseudo-PPS products of 10 rainfall events in Table 1. The solid lines represent the ordinary least square regression fits. The smaller scale ratios (λ = 1, 2) are excluded in the regression analysis.

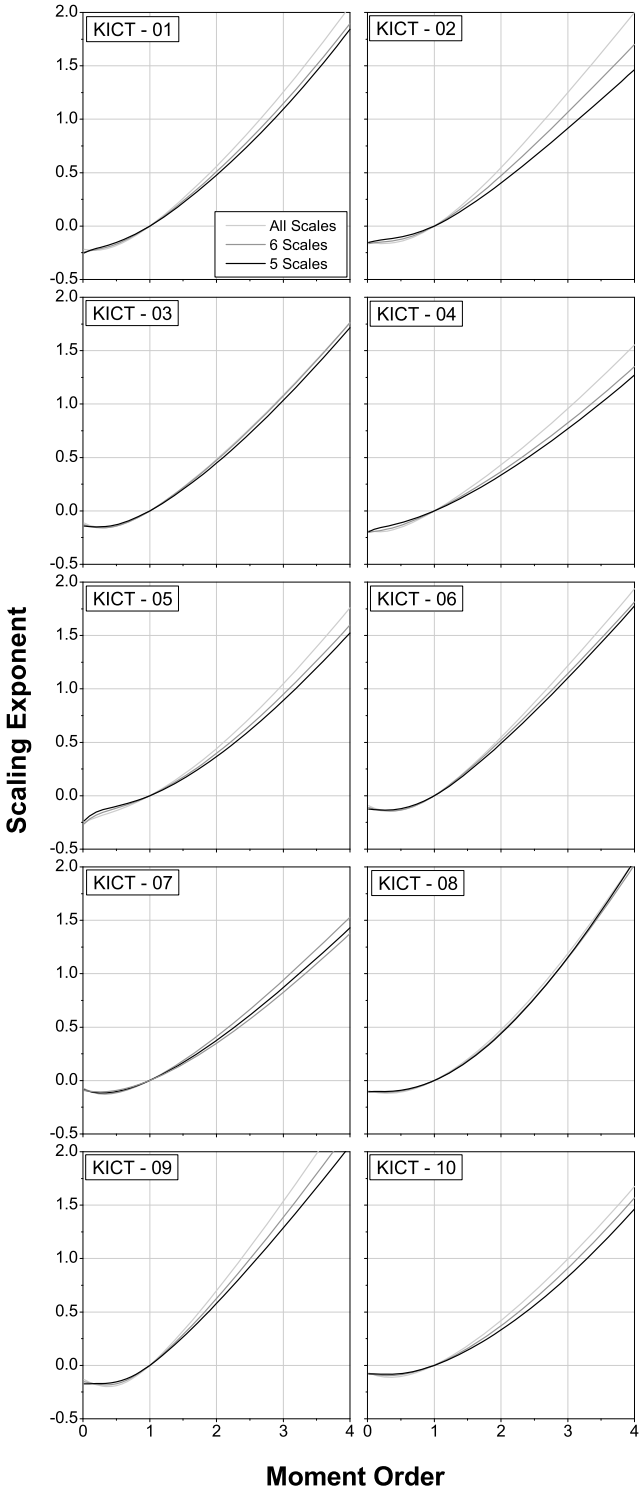

Figure 8. Moment scaling exponents plotted against the moment order q for the Pseudo-PPS products of 10 rainfall events in Table 1. Each panel compares the scaling exponents obtained for three scenarios: (1) when all the scale ratios (λ) in Figure 6 are included in regression, (2) when $\lambda = 1$ is excluded, and (3) when $\lambda = 1, 2$ are excluded.

section 4.3. In Figure 10, the DTM analysis is shown for the PPPS products of the rainfall events KICT-06 and KICT-08. The top frames of Figure 10 show the double trace moments (estimated using equation (8)) plotted against the scale ratio λ for different moment orders η and for a fixed q value of 1.6. The double trace moments displayed log-log linearity

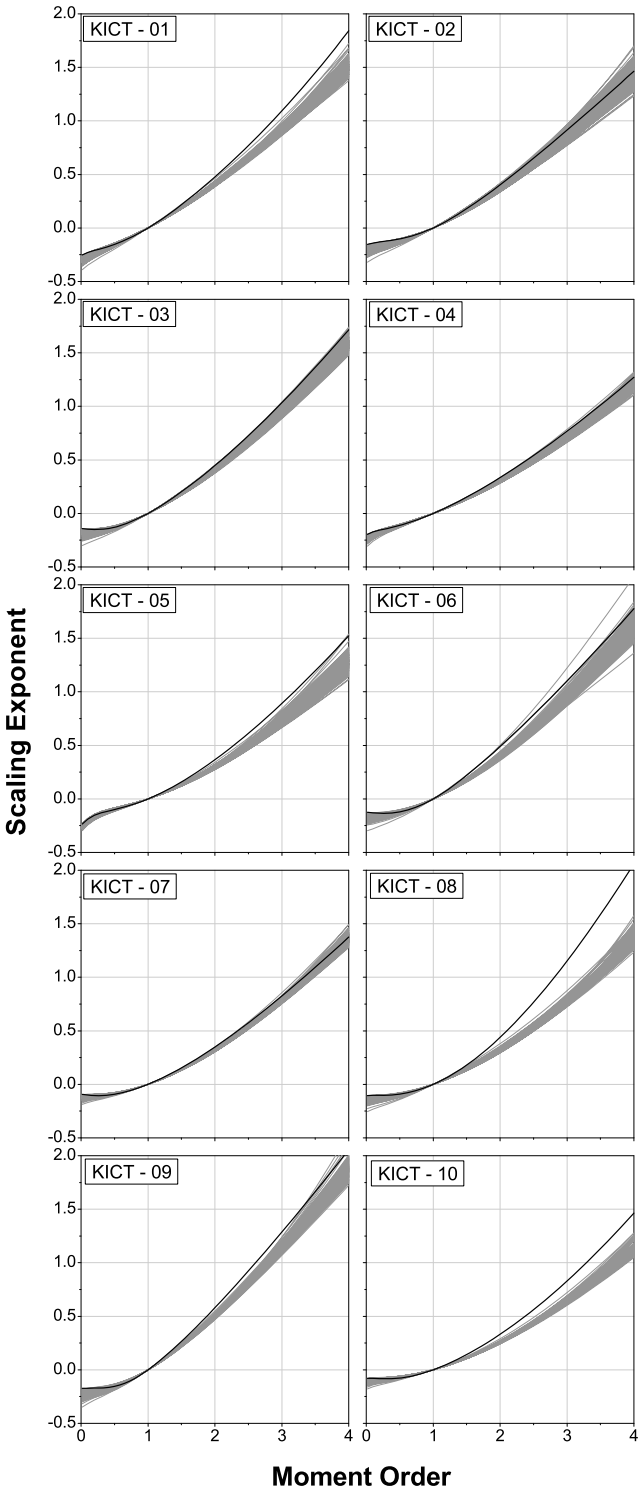

Figure 9. Same as in Figure 4, but for the moment scaling exponents.

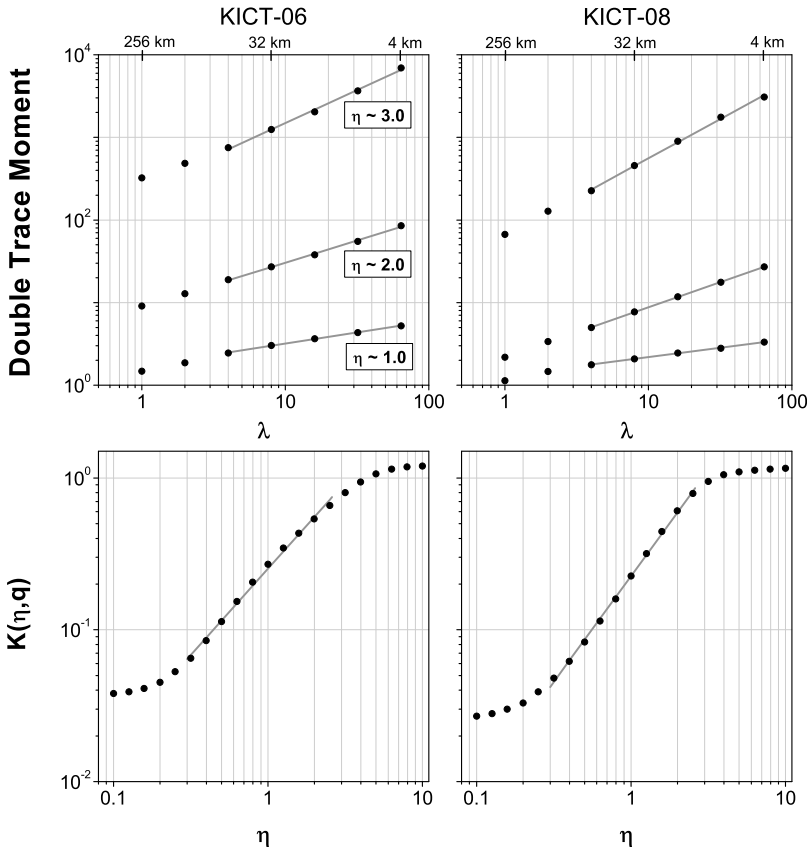

Figure 10. (top) Scaling of double trace moments (moment order q = 1.6) with respect to the scale ratio for the two rainfall events. The solid lines show the ordinary least squares regression fit (the first two points are not considered in regression). (bottom) Scaling of the double trace moment exponents with respect to the moment order η. The solid lines show the ordinary least squares regression fit (the first 5 and last 6 points are not considered in regression).

with the scale ratio λ for various η values (Figure 10, top). We obtained the slopes $K(q,\eta)$ in equation (9) by performing ordinary least squares regression, excluding the moment value corresponding to the lowest value of λ. The slope of $K(q,\eta)$ plotted against η in the double logarithmic plot (Figure 10, bottom) gives the value of the multifractality index α. The intermittency parameter C_1 was obtained by using equations (5) and (10) for a fixed q. In this study, we carried out the DTM analysis for q equal to 1.2, 1.6, 2.0, and 2.4 and estimated the average UM model parameters α and C_1. Figure 11 shows the moment scaling exponents (solid dots) and the DTM-fitted moment scaling functions (gray lines) for the PPPS RR products of all 10 rainfall events.

[38] The values of universal multifractal model parameters for all 10 rainfall events and for both the algorithms (PPPS and Hi-Fi) are listed in Table 4. Similar to the correlation and power spectrum analysis, the UM model parameters were not significantly different for the PPPS and Hi-Fi products (Table 4). The intermittency parameter for the PPPS product ranged from 0.21 for the event KICT-10 to 0.40 for KICT-09, whereas the multifractality index varied from 0.99 for KICT-01 to 1.39 for KICT-08 (Table 4). From the low value of C_1 and the relatively high value of α for the storm KICT-10 (Table 4), we can say that the storm is more space-filling and has relatively fewer spikes than the other storms; the result is consistent with correlation and power spectrum analysis. Similarly, the high value of C_1 and relatively low value of α for the KICT-09 suggest that the storm is spikier and less space-filling than other storms.

[39] We performed the DTM analysis for all 200 probable rainfall fields and compared the UM model parameters with those of the PPPS product to assess the impact of RR errors (Table 4). In general (except C_1 for KICT-02 and α for KICT-07), the UM model parameters for the PPPS product are greater than the corresponding average values estimated from probable rainfall events (Table 4). The higher value of C_1 for the PPPS product meant an increase in the intermittency or a decrease in the smoothness of the field, which is contradictory to the result obtained from the correlation and power spectrum analysis. However, it can be explained by focusing on the behavior of α. Table 4 illustrates that the value of α for the PPPS product is greater than the average α from probable rainfall events, which means fewer spikes and smoother fields. The net effect is the smoothing of the field and is therefore consistent with the correlation and power spectrum analysis.

[40] The explanation provided in the previous paragraph must be taken with caution as C_1 and α for the PPPS product

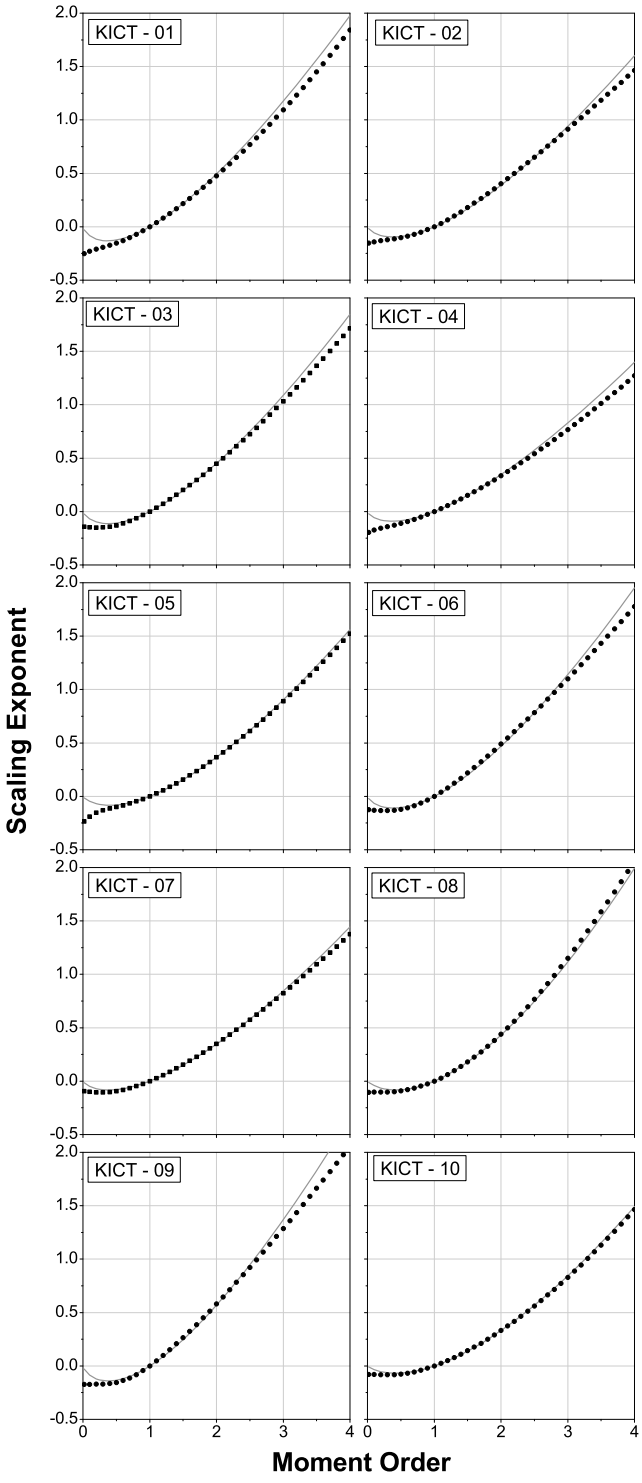

Figure 11. Moment scaling functions (solid lines) fitted to the scaling exponents (dots) using the double trace moment technique.

lie within the 90% confidence interval for some of the selected storms. For example, although C_1 and α for storms KICT-03 and KICT-06 are greater than corresponding average values from probable rainfall events, they lie within the 5th and 95th percentile of the distribution obtained from the probable rainfall events (Table 4). At the 10% significance level, there is not enough evidence that the UM parameters are overestimated for KICT-03 and KICT-06. We then estimated the Hurst exponent H using equation (7) for the RR products as well as the probable rainfall events (Table 5). The Hurst exponent for the PPPS products is larger than the 95th percentile for all of the storms. As the Hurst exponent characterizes the degree of smoothness, the effect of RR errors is to increase the smoothness of the rainfall fields. Since the power spectrum slope was used in the computation of the Hurst exponent, any impact of errors on β propagated into the estimation of the Hurst exponent.

6. Summary and Conclusions

[41] Remotely sensed rainfall products, which are widely used for the spatial and temporal characterization of rainfall events, are affected by errors from various sources. Therefore, it is imperative to quantify the effect of errors on the estimated rainfall characteristics. In this study, we investigated the impact of radar-rainfall (RR) estimation errors on the spatial characterization of RR products for warm season rainfall events over Wichita, Kansas. For each storm, we generated 200 probable rainfall events using the rainfall generator developed by *Villarini et al.* [2009a] that was based on a recent RR error model of *Ciach et al.* [2007]. We assessed the effect of errors on different spatial characterization tools such as the spatial correlation function, power spectrum, and moment scaling function. Besides performing qualitative analysis, we also quantified the impact of errors by parameterizing the aforementioned functions with models widely used in the rainfall literature.

[42] From the spatial correlation analysis, we found that the shape parameter, which characterizes the behavior of the spatial correlation function at the small separation lags, was significantly overestimated for the RR products of all of the storms. In general, there was a tendency for the correlation distance (defined as the distance at which the correlation drops to $1/e$) to be also overestimated for the RR products. The power spectrum analysis revealed that RR estimation errors would smooth the fields at higher frequencies, leading to the overestimation of the power spectrum slope for 8 of 10 rainfall events. The correlation and power spectrum analysis also showed that the effect of RR errors was the smallest for the more variable events. Moment scaling analysis was then carried out to see the effect of errors on the scaling of statistical moments of various orders. The moment scaling functions were fitted with a universal multifractal model using the double trace moment (DTM) technique. The results from the DTM analysis also suggested smoothing of rainfall fields by the RR errors. However, the results were not as conclusive as the correlation and power spectrum analysis for some of the rainfall events. The Hurst exponent, which characterizes the degree of nonconservation or smoothness in the rainfall fields, was also significantly overestimated for all of the storm events.

[43] Radar-rainfall fields have been used in several studies to infer spatial characteristics of the underlying unknown areal rainfall fields. However, the effects of errors in the radar-rainfall fields on the inferred statistics have always

Table 4. Parameters of the Universal Multifractal Model Estimated Using the Double Trace Moment Technique From the Radar-Rainfall Data Obtained From Pseudo-PPS (PPPS) and Hi-Fi Algorithms[a]

	Intermittency Parameter C_1					Multifractality Exponent α				
			Probable Rainfall					Probable Rainfall		
Storm ID	PPPS	Hi-Fi	$Q_{0.05}$	Mean	$Q_{0.95}$	PPPS	Hi-Fi	$Q_{0.05}$	Mean	$Q_{0.95}$
KICT-01	0.36	0.37	0.31	0.32	0.35	0.99	0.99	0.80	0.89	0.96
KICT-02	0.27	0.28	0.25	0.28	0.32	1.09	1.07	0.86	0.98	1.08
KICT-03	0.32	0.32	0.28	0.31	0.34	1.07	1.05	0.93	1.02	1.09
KICT-04	0.25	0.26	0.22	0.23	0.25	1.02	1.03	0.94	1.01	1.06
KICT-05	0.25	0.25	0.20	0.21	0.23	1.18	1.17	1.07	1.15	1.22
KICT-06	0.32	0.33	0.26	0.29	0.33	1.12	1.11	1.00	1.11	1.20
KICT-07	0.24	0.26	0.21	0.22	0.23	1.12	1.11	1.13	1.19	1.25
KICT-08	0.27	0.28	0.21	0.23	0.27	1.39	1.39	1.03	1.15	1.25
KICT-09	0.40	0.42	0.34	0.37	0.40	1.07	1.02	0.94	1.03	1.11
KICT-10	0.21	0.21	0.16	0.18	0.19	1.33	1.31	1.13	1.24	1.33

[a]The table also shows the mean and 5th and 95th percentiles of the corresponding parameters for the probable rainfall fields. All of the parameters are estimated for hourly accumulations with the spatial resolution 4 km.

been studied using arbitrary error models. The main strength of our study lies in the use of a recently developed RR error model and rainfall generator, whose parameters were derived from 6 years of high-quality datasets. Overall, the results from our study indicate that the systematic and random errors in the RR fields lead to significant overestimation of the spatial characteristics, particularly at the smallest scales. The results are in agreement with previous studies using arbitrary models of RR errors. The study provides quantitative information regarding the effect of RR errors on the estimated correlation functions, power spectrum, and scaling functions. Such information is of great value when trying to build parsimonious models of rainfall based on aforementioned spatial properties. Also, by propagating the errors through hydrologic models, we can quantify the role of RR errors in characterizing the hydrologic response.

[44] In this study, we have focused on the spatial structure of rainfall events. The investigation of the effect of radar-rainfall errors on the space-time characteristics of rainfall would require inclusion of the temporal dependencies of the random errors into the generator developed by *Villarini et al.* [2009a], which is beyond the scope of this study.

Table 5. Hurst Exponent Estimated Using Equation (7) for the Radar-Rainfall Data Obtained From Pseudo-PPS (PPPS) and Hi-Fi Algorithms[a]

	Hurst Exponent H				
			Probable Rainfall		
Storm ID	PPPS	Hi-Fi	$Q_{0.05}$	Mean	$Q_{0.95}$
KICT-01	0.50	0.51	0.28	0.35	0.40
KICT-02	0.56	0.57	0.28	0.36	0.43
KICT-03	0.35	0.35	0.21	0.26	0.30
KICT-04	0.55	0.56	0.32	0.38	0.43
KICT-05	0.54	0.55	0.31	0.37	0.43
KICT-06	0.27	0.30	0.11	0.17	0.23
KICT-07	0.55	0.56	0.35	0.40	0.44
KICT-08	0.50	0.52	0.22	0.28	0.35
KICT-09	0.33	0.32	0.19	0.24	0.29
KICT-10	0.61	0.63	0.31	0.37	0.43

[a]The table also shows the mean and 5th and 95th percentiles of the corresponding parameters for the probable rainfall fields. All the parameters are estimated for hourly accumulations with the spatial resolution 4 km.

[45] **Acknowledgments.** Development of Hydro-NEXRAD was supported with by the National Science Foundation award ATM 0427422. Storm analysis was conducted as part of flood research supported by the National Science Foundation grant EAR-0450320. Authors would also like to acknowledge the support by the TeraGrid grant TG-EAR090037T. Gabriele Villarini was supported by NASA Headquarters under the Earth Science Fellowship grant NNX06AF23H while a graduate student at the University of Iowa. The fourth author also acknowledges partial support of the Rose and Joseph Summers endowment.

References

Bacchi, B., and N. T. Kottegoda (1995), Identification and calibration of spatial correlation patterns of rainfall, *J. Hydrol.*, *165*, 311–348.

Bell, T. L., and P. K. Kundu (1996), A study of the sampling error in satellite rainfall estimates using optimal averaging of data and a stochastic model, *J. Climate*, *9*, 1251–1268.

Bell, T. L., A. Abdullah, R. L. Martin, and G. R. North (1990), Sampling errors for satellite-derived tropical rainfall – Monte Carlo study using a space-time stochastic model, *J. Geophys. Res.*, *95*(D3), 2195–2205, doi:10.1029/JD095iD03p02195.

Berndtsson, R. (1988), Temporal variability in the spatial correlation of daily rainfall, *Water Resour. Res.*, *24*(9), 1511–1517, doi:10.1029/WR024i009p01511.

Ciach, G. J., and W. F. Krajewski (2006), Analysis and modeling of spatial correlation structure in small-scale rainfall in central Oklahoma, *Adv. Water Resour.*, *29*, 1450–1463.

Ciach, G. J., W. F. Krajewski, and G. Villarini (2007), Product error-driven uncertainty model for probabilistic quantitative precipitation estimation with NEXRAD data, *J. Hydrometeorol.*, *8*, 1325–1347.

Crum, T. D., and R. L. Alberty (1993), The WSR-88D and the WSR-88D operational support facility, *Bull. Am. Meteorol. Soc.*, *74*, 1669–1687.

Fulton, R. A., J. P. Breidenbach, D.-J. Seo, and D. A. Miller (1998), The WSR-88D rainfall algorithm, *Weather Forecast.*, *13*, 377–395.

Gagnon, J.-S., S. Lovejoy, and D. Schertzer (2006), Multifractal Earth topography, *Nonlinear Proc. Geophys.*, *13*, 541–570.

Gebremichael, M., and W. F. Krajewski (2004), Assessment of statistical characterization of small scale variability from radar: analysis of TRMM ground validation datasets, *J. Appl. Meteorol.*, *43*, 1180–1199.

Gebremichael, M., W. F. Krajewski, M. Morrissey, G. Huffman, and R. Adler (2005), A detailed evaluation of GPCP one-degree daily rainfall estimates over the Mississippi River Basin, *J. Appl. Meteorol.*, *44*, 665–681.

Gebremichael, M., W. F. Krajewski, T. M. Over, Y. N. Takayabu, P. Arkin, and M. Takayabu (2008), Scaling of tropical rainfall as observed by TRMM precipitation radar, *Atmos. Res.*, *88*, 337–354.

Germann, U., M. Berenguer, D. Sempere-Torres, and M. Zappa, M. (2009), REAL – ensemble radar precipitation for hydrology in a mountainous region, *Q. J. R. Meteorol. Soc.*, *135*, 445–456.

Gupta, V. K., and E. C. Waymire (1993), A statistical analysis of mesoscale rainfall as a random cascade, *J. Appl. Meteorol.*, *32*, 251–267.

Harris, D., A. Seed, M. Menabde, and G. Austin (1997), Factors affecting multiscaling analysis of rainfall time series, *Nonlinear Proc. Geophys.*, *4*, 137–155.

Harris, D., E. Foufoula-Georgiou, and C. Kummerow (2003), Effects of underrepresented hydrometeor variability and partial beam filling on microwave brightness temperatures for rainfall retrieval, *J. Geophys. Res.*, *108*(D8), 8380, doi:10.1029/2001JD001144.

Hubert, P., Y. Tessier, S. Lovejoy, D. Schertzer, P. Ladoy, J. P. Carbonnel, and S. Violette (1993), Multifractals and extreme rainfall events, *Geophys. Res. Lett.*, *20*(10), 931–934, doi:10.1029/93GL01245.

Jordan, P. W., A. W. Seed, and P. E. Weinmann (2003), A stochastic model of radar measurement errors in rainfall accumulations at catchment scale, *J. Hydrometeorol.*, *4*(5), 841–855.

Kirstetter, P.-E., G. Delrieu, B. Boudevillain, and C. Obled (2010), Toward an error model for radar quantitative precipitation estimation in the Cévennes-Vivarais region, France, *J. Hydrology*, doi:10.1016/j.jhydrol.2010.01.009, in press.

Klazura, G. E., and D. A. Imy (1993), A description of the initial set of analysis products available from the NEXRAD WSR-88D system, *Bull. Am. Meteorol. Soc.*, *74*, 1293–1311.

Krajewski, W. F., and J. A. Smith (2002), Radar hydrology: Rainfall estimation, *Adv. Water Resour.*, *25*(8–12), 1387–1394.

Krajewski, W. F., E. N. Anagnostou, and G. J. Ciach (1996), Effect of radar observation process on the inferred rainfall statistics, *J. Geophys. Res.*, *101*(D21), 26,493–26,502, doi:10.1029/96JD01616.

Krajewski, W. F., G. J. Ciach, and E. Habib (2003), An analysis of small-scale rainfall variability in different climatological regimes, *Hydrolog. Sci. J.*, *48*(2), 151–162.

Krajewski, W. F., et al. (2010), Towards better utilization of NEXRAD data in hydrology: An overview of Hydro-NEXRAD, *J. Hydroinformatics*, doi:10.2166/hydro.2010.056, in press.

Lavallee, D., S. Lovejoy, D. Schertzer, and P. Ladoy (1993), Nonlinear variability and landscape topography: analysis and simulation, in *Fractals in Geography*, edited by L. De Cola and N. Lam, pp. 158–192, Prentice Hall, Englewood Cliffs, NJ.

Lazarev, A., D. Schertzer, S. Lovejoy, and Y. Chigirinskaya (1994), Multifractal analysis of tropical turbulence: Part II. Vertical scaling and generalized scale invariance, *Nonlinear Proc. Geophys.*, *1*, 115–123.

Liu, H. H., and F. J. Molz (1997), Multifractal analysis of hydraulic conductivity distributions, *Water Resour. Res.*, *33*(11), 2483–2488, doi:10.1029/97WR02188.

Lovejoy, S., and D. Schertzer (2006), Multifractals, cloud radiances and rain, *J. Hydrol.*, *322*, 59–88.

Lovejoy, S., D. Schertzer, and V. C. Allaire (2008), The remarkable wide range spatial scaling of TRMM precipitation, *Atmos. Res.*, *90*, 10–32.

Mandapaka, P. V., W. F. Krajewski, G. J. Ciach, G. Villarini, and J. A. Smith (2009a), Estimation of radar-rainfall error spatial correlation, *Adv. Water Resour.*, *32*, 1020–1030.

Mandapaka, P. V., P. Lewandowski, W. E. Eichinger, and W. F. Krajewski (2009b), Multiscaling analysis of high resolution space-time lidar rainfall, *Nonlinear Proc. Geophys.*, *16*, 579–586.

Marsan, D., D. Schertzer, and S. Lovejoy (1996), Causal space-time multifractal modelling of rain, *J. Geophys. Res.*, *31*, 333–346, doi:10.1029/96JD01840.

McCollum, J. R., W. F. Krajewski, R. R. Ferraro, and M. B. Ba (2002), Evaluation of biases of satellite rainfall estimation algorithms over the continental United States, *J. Appl. Meteorol.*, *41*(11), 1065–1080.

Menabde, M., A. Seed, D. Harris, and G. Austin (1997), Self-similar random fields and rainfall simulation, *J. Geophys. Res.*, *102*(D12), 13,509–13,515, doi:10.1029/97JD00915.

Morales, J. E., and G. Poveda (2009), Diurnally driven scaling properties of Amazonian rainfall fields: Fourier spectra and order-q statistical moments, *J. Geophys. Res.*, *114*, D11104, doi:10.1029/2008JD011281.

Naud, C., D. Schertzer, and S. Lovejoy (1996), Fractional integration and radiative transfer in multifractal atmospheres, in *Stochastic Models in Geosystems*, edited by W. Woyczynski and S. Molchansov, pp. 239–267, Heidelberg: Springer-Verlag, New York, Berlin.

Nicholson, S. (1986), Spatial coherence of African rainfall anomalies: Interhemispheric teleconnections, *J. Climate Appl. Meteorol.*, *25*, 1365–1381.

Ntelekos, A. A., J. A. Smith, M.-L. Baeck, W. F. Krajewski, A. J. Miller, and R. Goska (2008), Extreme hydrometeorological events and the urban environment: Dissecting the 7 July 2004 thunderstorm over the Baltimore, MD, metropolitan region, *Water Resour. Res.*, *44*, W08446, doi:10.1029/2007WR006346.

Ntelekos, A. A., J. A. Smith, L. J. Donner, J. D. Fast, W. I. Gustafson Jr., E. G. Chapman, and W. F. Krajewski (2009), The effects of aerosols on intense convective precipitation in the northeastern US, *Q. J. R. Meteorol. Soc.*, *135*, 1367–1391.

Nykanen, D. K. (2008), Linkages between orographic forcing and the scaling properties of convective rainfall in mountainous regions, *J. Hydrometeorol.*, *9*, 327–347.

Nykanen, D. K., and D. Harris (2003), Orographic influences on the multiscale statistical properties of precipitation, *J. Geophys. Res.*, *108*(D8), 8381, doi:10.1029/2001JD001518.

Perica, S., and E. Foufoula-Georgiou (1996), Linkage of scaling and thermodynamic properties of rainfall: Results from midlatitude mesoscale convective systems, *J. Geophys. Res.*, *101*(D3), 7431–7448, doi:10.1029/95JD02372.

Purdy, J. C., D. Harris, G. L. Austin, A. W. Seed, and W. Gray (2001), A case study of orographic rainfall processes incorporating multiscaling characterization techniques, *J. Geophys. Res.*, *106*, 7837–7845, doi:10.1029/2000JD900622.

Ricciardulli, L., and P. D. Sardeshmukh (2002), Local time- and space scales of organized tropical deep convection, *J. Climate*, *15*(19), 2775–2790.

Schertzer, D., and S. Lovejoy (1987), Physical modeling and analysis of rain and clouds by anisotropic scaling multiplicative processes, *J. Geophys. Res.*, *92*(D8), 9693–9714, doi:10.1029/JD092iD08p09693.

Schmitt, F., D. Schertzer, S. Lovejoy, and G. Brunet (1994), Estimation of universal multifractal indices for atmospheric turbulent velocity fields, *Fractals*, *1*, 569–575.

Schmitt, F., D. Schertzer, S. Lovejoy, and G. Brunet (1996), Universal multifractal structure of atmospheric temperature and velocity fields, *Europhys. Lett.*, *34*, 195–200.

Seo, B.-C., W. F. Krajewski, A. Kruger, P. Domaszczynski, M. Steiner, and J. A. Smith (2009), Radar-rainfall estimation algorithms of Hydro-NEXRAD, *J. Hydroinformatics*, in press.

Smith, J. A., D.-J. Seo, M. L. Baeck, and M. D. Hudlow (1996), An intercomparison study of NEXRAD precipitation estimates, *Water Resour. Res.*, *32*(7), 2035–2045, doi:10.1029/96WR00270.

Smith, T. M., P. A. Arkin, J. J. Bates, and G. J. Huffman (2006), Estimating bias of satellite-based precipitation products, *J. Hydrometeorol.*, *7*, 841–856.

Sumner, G. N. (1982), The spatial organization of daily rainfall in eastern New South Wales, *Int. J. Climatol.*, *3*, 361–374.

Stauffer, F. (2005), Uncertainty estimation of path lines in groundwater models, *Ground Water*, *43*, 843–849.

Tchiguirinskaia, I., S. Lu, F. J. Molz, T. M. Williams, and D. Lavallee (2000), Multifractal versus monofractal analysis of wetland topography, *Stoch. Env. Res. Risk Assess.*, *14*, 8–32.

Tessier, Y., S. Lovejoy, and D. Schertzer (1993a), Universal multifractals in rain and clouds: theory and observations, *J. Appl. Meteorol.*, *32*, 223–250.

Tessier, Y., S. Lovejoy, D. Schertzer, D. Lavallee, and B. Kerman (1993b), Universal multifractal indices for the ocean surface at far red wavelengths, *Geophys. Res. Lett.*, *20*(12), 1167–1170, doi:10.1029/93GL00369.

Villarini, G., and W. F. Krajewski (2009a), Inference of spatial scaling properties of rainfall: Impact of radar-rainfall estimation uncertainties, *IEEE Geosci. Remote Sens. Lett.*, *6*, 812–815, doi:10.1109/LGRS.2009.2025891.

Villarini, G., and W. F. Krajewski (2009b), Empirically based modelling of uncertainties in radar rainfall estimates for a C-band weather radar at different time scales, *Q. J. R. Meteorol. Soc.*, *135*, 1424–1438.

Villarini, G., and W. F. Krajewski (2010a), Review of different sources of uncertainty in single polarization radar-based estimates of rainfall, *Surv. Geophys.*, *31*, 107–129.

Villarini, G., and W. F. Krajewski (2010b), Sensitivity studies of the models of radar-rainfall uncertainties, *J. Appl. Meteorol. Climatol.*, *49*, 288–309, doi:10.1175/2009JAMC2188.1.

Villarini, G., G. J. Ciach, W. F. Krajewski, K. M. Nordstrom, and V. K. Gupta (2007a), Effects of systematic and random errors on the spatial scaling properties in radar-estimated rainfall, in *Nonlinear Dynamics in Geosciences*, edited by A. A. Tsonis and J. Elsner, pp. 37–51, Springer, New York.

Villarini, G., J. B. Lang, F. Lombardo, F. Napolitano, F. Russo, and W. F. Krajewski (2007b), Impact of different regression frameworks on the estimation of the scaling properties of radar rainfall, *Atmos. Res.*, *86*, 340–349.

Villarini, G., P. V. Mandapaka, W. F. Krajewski, and R. J. Moore (2008), Rainfall and sampling errors: A rain gauge perspective, *J. Geophys. Res.*, *113*, D11102, doi:10.1029/2007JD009214.

Villarini, G., W. F. Krajewski, G. J. Ciach, and D. L. Zimmerman (2009a), Product error-driven generator of probable rainfall conditioned on WSR-88D precipitation estimates, *Water Resour. Res.*, *45*, W01404, doi:10.1029/2008WR006946.

Villarini, G., W. F. Krajewski, and J. A. Smith (2009b), New paradigm for statistical validation of satellite precipitation estimates: Application to a large sample of the TMPA 0.25-degree three hourly estimates over Oklahoma, *J. Geophys. Res.*, *114*, D12106, doi:10.1029/2008JD011475.

Villarini, G., W. F. Krajewski, A. A. Ntelekos, K. P. Georgakakos, and J. A. Smith (2010), Towards probabilistic forecasting of flash floods: The combined effects of uncertainty in radar-rainfall and flash flood guidance, *J. Hydrol.*, doi:10.1016/j.jhydrol.2010.02.014, in press.

W. F. Krajewski and B.-C. Seo, IIHR-Hydroscience and Engineering, University of Iowa, Iowa City, IA 52242, USA.

P. V. Mandapaka, MeteoSwiss, Via ai Monti 146, Locarno-Monti, CH-6605, Switzerland. (pradeep.mandapaka@meteoswiss.ch)

G. Villarini, Department of Civil and Environmental Engineering, Princeton University, Princeton, NJ 08540, USA.